



ELSEVIER

Available online at [www.sciencedirect.com](http://www.sciencedirect.com)

 ScienceDirect

Proceedings of the Combustion Institute 31 (2007) 757–764

Proceedings  
of the  
Combustion  
Institute

[www.elsevier.com/locate/proci](http://www.elsevier.com/locate/proci)

# Experimental evaluation of strategies for quantitative laser-induced-fluorescence imaging of nitric oxide in high-pressure flames (1–60 bar)

Tonghun Lee <sup>\*</sup>, Jay B. Jeffries, Ronald K. Hanson

*Mechanical Engineering Department, Stanford University, Stanford, CA 94305, USA*

## Abstract

Nitric oxide laser-induced-fluorescence (NO-LIF) 2-D imaging measurements using a new multi-spectral detection strategy are reported for high-pressure flames (1–60 bar). This work builds on previous research that identified interference LIF from O<sub>2</sub> and CO<sub>2</sub> in high-pressure flames and optimized the choice of excitation strategies as a function of application conditions. In this study, design rules are presented to optimize the LIF detection wavelengths for quantitative 2-D NO-LIF measurements over a wide range of pressures (1–60 bar) and temperatures. Simultaneous detection of LIF in multiple wavelength regions enables correction of the NO signal for interference from O<sub>2</sub> and CO<sub>2</sub> and allows simultaneous imaging of all three species. New experiments of wavelength-resolved 1-D LIF in slightly lean ( $\phi = 0.9$ ) and slightly rich ( $\phi = 1.1$ ) methane/air flames are used to evaluate the design rules and estimate the NO detection limits for a wide range of flame conditions. The quantitative 2-D measurements of NO in the burnt gas are compared with model calculations (using GRI-Mech 3.0) versus pressure for slightly lean and slightly rich flames. The discussions and demonstrations reported in this study provide a practical guideline for application of instantaneous 1-D or 2-D NO-LIF imaging strategies in high-pressure combustion systems.

© 2006 The Combustion Institute. Published by Elsevier Inc. All rights reserved.

*Keywords:* Nitric oxide; Laser-induced fluorescence; NO reburn; Combustion diagnostics

## 1. Introduction

The unique properties of laser light enable selective and quantitative probing of many chemical species with high temporal and spatial resolution in combustion environments [1,2]. A species of particular concern for its harmful impact on the environment is nitric oxide (NO), whose formation

mechanisms have been extensively studied and documented in the literature [3,4]. Experimentally, UV laser-induced-fluorescence (LIF) of NO, including single point, 1-D line imaging and 2-D planar imaging, is a well-established tool for understanding NO formation in practical combustion systems as well as laboratory flames. NO-LIF measurements to date have mostly used the *A-X* system with transitions in the (0,0), (0,1) or the (0,2) bands at 226, 235 and 248 nm, respectively [5–7]. Some measurements have been made in the *D-X*(0,1) band at 193 nm [8], though the *D-X* measurements often experience limited success due to transmission problems in hot combustion environments.

<sup>\*</sup> Corresponding author. Current address: Department of Mechanical Engineering, Michigan State University. Fax: +1 517 353 1750.

*E-mail address:* [tonghun@egr.msu.edu](mailto:tonghun@egr.msu.edu) (T. Lee).

More importantly, the elevated pressures of combustion environments in most practical systems introduce significant complications in the application of NO-LIF, and many of these difficulties were identified a decade ago [9–12]. Recently, we began a comprehensive study of quantitative NO-LIF in flames up to 60 bar, leading to enhanced understanding of high-pressure NO-LIF. In this previous work, different *excitation* strategies were investigated and optimized excitation wavelengths for NO-LIF were recommended for various combustion environments [13–15].

In the present study, we introduce a new multi-spectral *detection* strategy for quantitative 2-D NO-LIF imaging. While the spectral analysis method is routinely used in bio-chemistry assays for complex polyatomic molecules, to our knowledge, this is the first application of multi-spectral detection in combustion LIF and certainly the first time for NO-PLIF diagnostics. This work builds on the results of our previous effort, and leads to a new strategy based on the use of multiple detection wavelength regions for simultaneous determination of NO and the interference from O<sub>2</sub> and CO<sub>2</sub> LIF. Design rules are developed and the detection wavelength regions or “windows” are optimized, using new wavelength-resolved 1-D NO-LIF experiments in slightly fuel lean ( $\phi = 0.9$ ) and slightly fuel rich ( $\phi = 1.1$ ) methane/air flames. Demonstration measurements of 2-D LIF imaging are then performed to validate the imaging strategy and estimate the NO detection limits for lean and rich high-pressure flames. Quantitative measurements of NO in these seeded flames are compared with detailed chemical kinetics calculations as a function of pressure and stoichiometry, and good agreement is observed within the limits imposed on the calculation by the uncertainty in the measured temperature.

## 2. Experimental

The apparatus used in this study has been previously described [13–15] and is only briefly discussed here. Laminar, premixed methane/air flat-flames at pressures from 1–60 bar were stabilized on a porous, sintered stainless matrix of 8 mm diameter. This burner was mounted in a pressurized vessel with an inner diameter of 60 mm with stabilization to  $\pm 0.1$  bar. Investigations were conducted for  $\phi = 0.9$  and 1.1 methane/air equivalence ratios. Optical access to the flame was possible via four quartz windows (Heraeus, Suprasil 2 Grade). Laser pulse energy ranged from 0.8–1.2 mJ/pulse (7 ns pulse at 10 Hz with linewidth of  $0.2 \text{ cm}^{-1}$ ) from a Nd:YAG-pumped (Quanta Ray GCR250) frequency-doubled (BBO) dye laser (LAS, LDL205). For spectrally resolved 1-D line imaging measurements, the beam was weakly focused

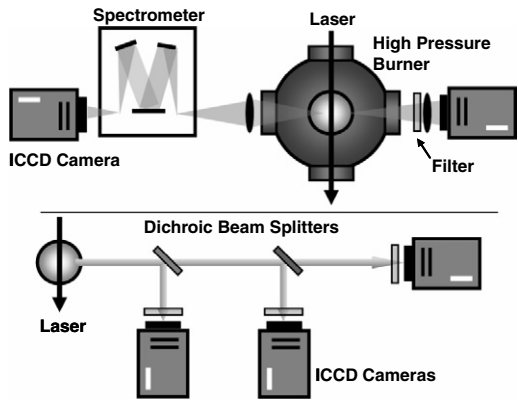


Fig. 1. Experimental setup for spectrally dispersed 1-D line-imaging (upper panel, left section) and spatially resolved 2-D imaging (upper panel, right section). Lower panel shows concept of multi-window detection scheme for practical applications.

(diameter = 1 mm) along a line 3 mm above the burner matrix and crosses the flame horizontally (Fig. 1, upper panel, left side). The pulse energy was monitored with a fast photodiode (LaVision). Fluorescence signals were collected at right angles to the laser beam and focused with a  $f = 105$  mm,  $f/4.5$  achromatic UV-lens (Nikon), dispersed spectrally through an imaging spectrometer (LaVision Chromex 250IS) and imaged onto an intensified CCD camera (LaVision Dynamight). For 2-D imaging measurements, the laser was optically stretched into a vertical sheet ( $0.5 \times 15$  mm) and imaged directly using an ICCD camera with different filter sets for suppression of Rayleigh Scattering and bandpass filtering (Fig. 1, upper panel, right side). The signals from 20 laser pulses were accumulated on chip for all measurements. For multi-window imaging measurements, wavelength regions were isolated with bandpass filters (discussed below) and separately collected on a single camera. For practical 2-D imaging applications where all spectral windows require simultaneous detection, a single laser, multi-camera strategy is proposed as shown in the lower section of Fig. 1.

## 3. Measurement strategy

### 3.1. High-pressure issues with NO-LIF

There are three significant complications that arise when applying NO-LIF to high-pressure combustion environments: (1) pressure broadening and shifting of NO transitions, (2) strong attenuation of UV light and (3) interference LIF. Excitation features of NO broaden with increased pressure, and for pressures greater than 10 bar, it is no longer possible to excite single

rotational features of the excitation spectrum due to the spectral overlap [15]. Along with an increase in fluorescence quenching of the NO  $A$  state, pressure broadening leads to a decrease in the overall signal strength since the laser linewidth ( $0.2 \text{ cm}^{-1}$ ) is less than the broadened linewidths. Second is the strong attenuation effect of both the excitation laser light and fluorescence signal. UV light at short wavelengths ( $<250 \text{ nm}$ ) is strongly absorbed in hot post-combustion gases, due mainly to strong absorption by  $\text{CO}_2$  and  $\text{H}_2\text{O}$  [16,17] ( $\text{CO}_2$  being the more dominant contributor in our wavelength range and temperatures). This effect increases with pressure as densities of the absorbing species increase. Finally, there can be significant signal interference. The  $B^3\Sigma^- - X^3\Sigma^+$  Schumann–Runge bands of  $\text{O}_2$  are pervasive in the same excitation and detection region and can be a major interference source in fuel lean and non-premixed flames [10]. Recently identified  $\text{CO}_2$  broadband emission (200–450 nm) is also a concern in high-pressure flames [18]. Additionally, polycyclic aromatic hydrocarbon (PAH) LIF emission can be a source of significant interference in fuel rich flames.

### 3.2. 2-D imaging of NO using multi-wavelength detection

Isolation of NO-LIF signal from interference sources, mainly from LIF of hot  $\text{O}_2$  and  $\text{CO}_2$  is investigated using LIF detection in multiple wavelength windows, a novel concept in NO-LIF imaging. While an ultimate goal of our work is the development of a single-shot 2-D imaging strategy, all the data presented here are obtained by accumulating multiple laser pulses on an ICCD camera (20 shots/image), made possible by the steady nature of our test flame. By averaging over multiple laser pulses, we are able to estimate the single-shot LIF signals achievable using lasers above the modest power range (0.8–1.2 mJ/pulse) of our current setup. Figure 2 shows a typical emission spectrum of NO-LIF using 1-D imaging with  $A-X(0,0)$  band excitation, where non-linear fitting and computational simulation of NO,  $\text{O}_2$  and  $\text{CO}_2$  LIF emission [19] are used to separate the spectrum into components from NO,  $\text{O}_2$ , and  $\text{CO}_2$  LIF, and the Rayleigh scattering of the laser. It can be seen that  $\text{O}_2$  and  $\text{CO}_2$  LIF are emitted throughout the entire region of interest and overlap with the spectral features of NO. Details regarding the selection criteria for the wavelength windows in Fig. 2 will be discussed later in the Section 4.

The specific steps for high-pressure 2-D LIF image analysis are discussed. The raw images first are corrected for spherical aberration of the collection lens (Lavisision ‘Davis’ Distortion Correction Routine) and for any non-uniform energy

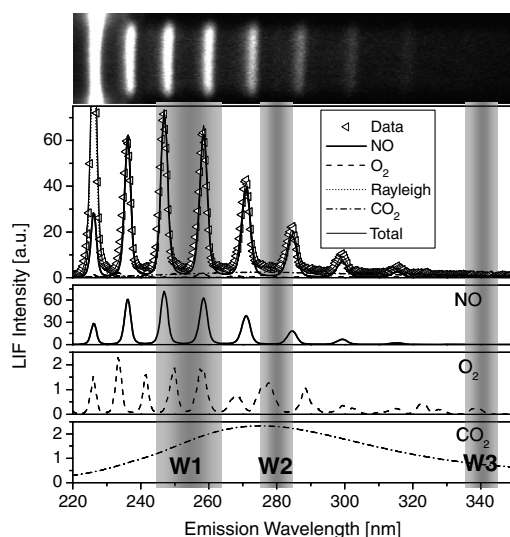


Fig. 2. Emission spectra of NO-LIF with 226.03 nm excitation (40 bar flame,  $\phi = 0.9$ , 300 ppm NO seeding). Spectra were obtained by taking 1-D line-imaging (top box). NO,  $\text{O}_2$  and  $\text{CO}_2$  emission profiles are enhanced for clarity (bottom 3 boxes). W1, W2 and W3 indicate the detection windows. Profiles were taken in a 1 mm region in the center of the flame.

distribution of the laser sheet. For each detection window, the signal at each pixel is the sum of contributions from NO,  $\text{O}_2$  and  $\text{CO}_2$  LIF. The fluorescence spectrum of each molecule is well-known [18,19] and provides the relative LIF signal strength for a particular molecule in the three detection windows. This knowledge, coupled with relative detection efficiencies of the filters in each window, allows us to solve for the NO,  $\text{O}_2$  and  $\text{CO}_2$  mole fractions. Pixel-by-pixel solution enables reconstruction of the LIF images for all species. The images are then corrected for attenuation of the excitation laser light and fluorescence signal, which is dominated by absorption from hot  $\text{CO}_2$  with a small contribution from hot  $\text{H}_2\text{O}$ ; note absorption contributions from NO and  $\text{O}_2$  are negligible in the flames studied here. Attenuation of the laser light and fluorescence signal are corrected on a pixel-by-pixel basis using Beer–Lambert’s Law and absorption coefficients known from shock tube measurements [16] and simple consideration of the geometry. These corrections require some knowledge of the local temperature because the  $\text{CO}_2$  and  $\text{H}_2\text{O}$  absorption coefficients are temperature dependent and the  $\text{CO}_2$  and  $\text{H}_2\text{O}$  number densities are obtained using an assumption of thermal equilibrium in the post-flame gas. Temperature information is also needed to correct for the temperature variation of the NO-LIF signal via the temperature dependence of the laser-excited ground state population, the spectral overlap between the

laser-spectral profile and NO absorption spectrum, and the fluorescence yield. These corrections for NO-LIF temperature dependence are small for the excitation wavelength used, and only an estimate would be needed for single-shot 2-D imaging applications. However in this study, quantitative temperature fields were obtained by 2-D 2-line NO-LIF thermometry [20]. For the current work, an excitation wavelength of 226.03 nm that excites band ( $P_1(23.5)$ ,  $Q_1 + P_2(14.5)$ ,  $Q_2 + R_2(20.5)$ ) in the  $A-X(0,0)$  band is used. This wavelength has been previously identified as optimal for maximum NO signal strength and minimum interference from  $O_2$ -LIF [10,13].

### 3.3. Spectrally resolved line-imaging of NO

Spectrally resolved 1-D imaging is obtained by aligning the laser beam parallel to the spectrometer slit, and the LIF signal is dispersed onto an ICCD camera. This camera image (top box in Fig. 2), has the position along the laser beam on the ordinate and the fluorescence wavelength on the abscissa. 1-D line-imaging provides increased SNR ratio due to higher laser intensity (beam vs. sheet), direct visualization of interference sources, and a more flexible selection of excitation/detection strategies since NO-LIF can be easily isolated from interferences. In addition, only a single laser and single camera detection setup is required. Previous demonstrations of 1-D line-imaging in both laboratory flames [15] and practical combustors [21] can be found in the literature.

### 3.4. Saturation and laser energy

With modern-day high-power, short pulse (<10 ns) lasers, LIF signal dependence on laser energy can show non-linear effects due to saturation of the excitation transition. In our 1-D line imaging experiments, we observed only a slight deviation from linear excitation when the laser spectral intensity ( $I_v$ ) reached  $\sim 30 \text{ W m}^{-2} \text{ s}^{-1}$  (1 mJ, 7 ns pulse @ 226.03 nm with  $0.2 \text{ cm}^{-1}$  bandwidth and a focused diameter of 1 mm) in an atmospheric pressure flame. As pressure is increased to the pressures of current interest, the rapid increase in the rotational energy transfer refills the depleted ground state while removing excess population in the upper excited state, thereby greatly extending the linear regime of NO-LIF. This population recycling effect enables the use of higher laser power for linear single-shot imaging in high-pressure environments (e.g., up to 20 mJ/pulse @ 20 bar for our setup) resulting in increased SNR ratios. For 2-D imaging measurements, significantly stronger laser pulses can be used since the laser beam is dispersed into a sheet and the spectral intensity is decreased.

## 4. Results and discussion

### 4.1. Detection wavelength window selection and NO quantification

Figure 2 shows the detection windows used for the 2-D imaging measurements (W1, W2 and W3). Window 1 (254 nm, FWHM 17.5 nm; Asahi Optics) is the primary detection channel for NO, chosen to optimize the NO-LIF signal, while window 2 (280 nm, FWHM 12 nm; Lambda Research Optics) and Window 3 (340 nm, FWHM 10 nm; Asahi Optics) are used to correct the signal for interference from  $O_2$  and  $CO_2$ , respectively. In addition, a 240 nm long-pass filter was used for additional suppression of the Rayleigh scattering. The selection rules for W1, the primary NO-LIF detection window, maximize the selectivity and intensity, while minimizing the contribution from Rayleigh scattering of the laser. The bandpass width should also be wide enough to avoid bias in the collection efficiency depending on the rotational levels excited [7]. For our test flame, optimization was carried out by taking the spectrally resolved line-imaged data (Fig. 2) and scanning a simulated Gaussian filter function (with varying spectral widths) throughout the fluorescence spectrum. An example from a 40 bar,  $\phi = 0.9$  flame is shown in Fig. 3, where the signal purity (fraction of the LIF signal from NO) and relative NO-LIF intensity are plotted as a function of center wavelength of the simulated filter. For detection windows W2 and W3, which are used to isolate interference LIF, the selection criteria require regions with maximum fractional contribution

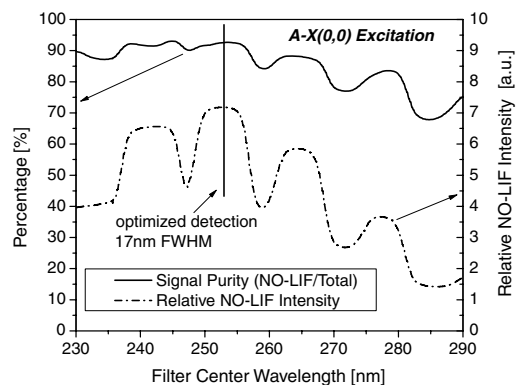


Fig. 3. Optimization of primary detection window W1 with  $A-X(0,0)$  excitation (40 bar,  $\phi = 0.9$  flame, 300 ppm NO seeding). Signal purity (fraction of LIF signal from NO) and relative NO-LIF intensity are plotted as a function of a simulated Gaussian filter function center wavelength (FWHM = 17 nm). Maximum signal purity and NO-LIF intensity can be obtained at a center wavelength of 254 nm.

from the specific interference species for increased accuracy in the correction.

While the 2-D imaging measurements reported in this paper primarily use the  $A-X(0,0)$  transition at 226.03 nm, optimization of the primary NO detection window W1 was also carried out for excitation using the  $A-X(0,1)$  and  $(0,2)$  transitions (235.873 and 247.941 nm), and the results are given in Table 1. Note that excitation using  $A-X(0,1)$  and  $(0,2)$  transitions offer the possibility of selecting W1 blue-shifted of the laser to avoid interference signals that occur at predominantly longer wavelengths. The same values for the detection windows W2 and W3 are recommended for all excitation strategies, as these windows are used to isolate  $O_2$  and  $CO_2$ , respectively.

Selection of the optimum number of detection wavelength windows requires knowledge regarding the global chemistry of the combustion process involved. For many experimental applications, single-window detection (W1) is sufficient as the flames have minimal  $O_2$  and  $CO_2$  interference if the proper excitation and fluorescence wavelengths are selected. Non-sooting flames with equivalence ratios near one or slightly richer, generally exhibit negligible levels of signals from  $O_2$ , and contribution from  $CO_2$  LIF can also be neglected for pressures less than 20 bar. For high-pressure flames ( $\geq 20$  bar) with lean chemistry ( $\phi < 0.9$ ), the interference from  $CO_2$  and  $O_2$  requires more than one detection window for sensitive and accurate detection of NO. In the case of rich flames ( $\phi > 1.5$ ) or flames with incomplete combustion of the fuel, interference from PAH and other hydrocarbons can additionally complicate NO-LIF measurements and will require further work to establish an appropriate detection strategy.

Quantification of NO-LIF intensities for 2-D imaging often requires an additional calibration measurement [22]. In practical applications such as engine measurements, a well-characterized flame may be inserted into the field of view for direct calibration of NO-LIF intensities [23]. This type of in situ calibration involves varying the amount of seeded NO and monitoring the corresponding change in the intensity of NO-LIF. Pre-

mixed lean flames are preferred to minimize NO reburn [22] in fuel rich-regions and to ensure that reburn rates depend linearly on seeding amounts. For the work presented here, NO-LIF signals are calibrated by varying the amounts of seeded NO at two different excitation wavelengths [24].

#### 4.2. Multi-window 2-D imaging of NO

Accurate 2-D NO-LIF images require corrections for various effects including laser and fluorescence signal attenuation, which vary with gas temperature. For steady laboratory flames, time consuming strategies such as multi-line NO-LIF fitting [24] can be used to obtain accurate 2-D temperature fields. For practical applications, 2-line thermometry offers a rapid means to obtain 2-D temperature images with relatively high precision. The temperature fields used in this study are obtained via 2-D 2-line thermometry of NO-LIF (line selection, 226.03 and 225.847 nm) and are shown in Fig. 4. A detection window centered at 254 nm (FWHM 17.5 nm; Asahi Optics) was used to maximize the signal purity of the NO-LIF.

Quantitative 2-D NO-LIF images obtained from the multi-window detection strategy are shown in Fig. 5. The data at pressures of 1 and 10 bar use a two-window (W1 and W2) detection since interference from  $CO_2$  is negligible under these conditions [18]. The second window provides a means to correct the raw image for the interference of  $O_2$ -LIF in slightly lean conditions ( $\phi = 0.9$ ). In slightly rich conditions ( $\phi = 1.1$ ),  $O_2$  is mostly consumed during the reaction and single-window (W1) detection is sufficient (NO-LIF signal selectivity  $> 98\%$ ) and no correction is needed. For pressures of 20 bar and higher, a three-window detection strategy is used for correction of the raw images for both  $O_2$  and  $CO_2$  LIF. The additional windows allow simultaneous images of hot  $CO_2$  and  $O_2$ . The data in Fig. 6 show the images of  $O_2$  and  $CO_2$  extracted from the interference signals for rich and lean 40 bar flames (right side) along with NO images with and without these corrections (left side). It should be noted that the impact of the correction on the NO intensity is not significant due to the fact that

Table 1  
Optimized selection for primary detection window W1 for  $A-X(0,0)$ ,  $(0,1)$  and  $(0,2)$  transitions

Excitation (nm)	Filter center $\lambda$	FWHM	Emission bands	NO fraction <sup>a</sup>	Rayleigh <sup>b</sup>
$A-X(0,0)$ 226	253	17	$A-X(0,2)$ , $(0,3)$	0.92	
$A-X(0,1)$ 235	226	8	$A-X(0,0)$	0.90	Yes
$A-X(0,1)$ 235	253	17	$A-X(0,2)$ , $(0,3)$	0.83	Yes
$A-X(0,1)$ 235	264	17	$A-X(0,3)$ , $(0,4)$	0.75	
$A-X(0,2)$ 248	226	10	$A-X(0,0)$	0.78	
$A-X(0,2)$ 248	235	8	$A-X(0,1)$	0.80	Yes

<sup>a</sup> NO fraction, NO-LIF signal/total signal ( $CH_4$ /air flame, 40 bar,  $\phi = 0.9$ , 300 ppm NO seeding).

<sup>b</sup> Refers to emission region which may be subject to interference from Rayleigh scattering of the laser.

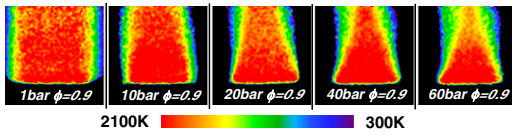


Fig. 4. NO temperature fields from 2-D 2-line NO-LIF thermometry (line selection, 226.03 nm and 225.847 nm) for various pressures (1–60 bar) at  $\phi = 0.9$ . Obtained by accumulating 20 shots on-chip and using 2-D PLIF imaging of NO-LIF.

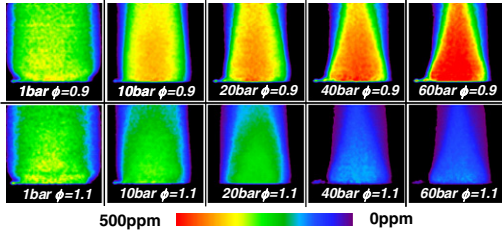


Fig. 5. Quantitative NO concentrations from multi-window 2-D NO-LIF Imaging (1–60 bar,  $\phi = 0.9$  and 1.1 with 300 ppm NO seeding). Note that the NO concentrations in rich flames are significantly reduced by NO reburn.

the excitation wavelength used has already been optimized for maximum suppression of the interference. The data in Fig. 5 show that for slightly lean flames ( $\phi = 0.9$ ), NO concentrations increase with pressure as predicted by the thermal and prompt NO formation mechanisms [3]. For slightly rich conditions ( $\phi = 1.1$ ), NO reburn due to excess hydrocarbons in the flame causes the concentrations to decrease with pressure.

The quantitative NO LIF data allows us to compare measurements of NO concentrations in the burnt gases (seeded NO) with model calculations. Figure 7 shows a comparison of NO concentrations obtained from NO-LIF imaging with computational calculations from a 1-D flame code using GRI-Mech 3.0 (Chemkin Premix from

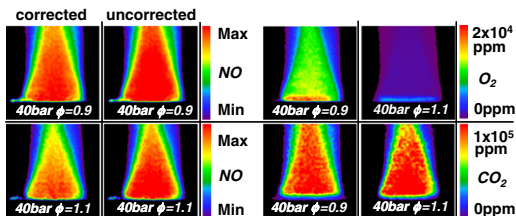


Fig. 6. NO, O<sub>2</sub> and CO<sub>2</sub> concentration fields from a three-window 2-D imaging strategy applied in a 40 bar flame ( $\phi = 0.9$  and 1.1 with 300 ppm NO seeding). For NO, interference-corrected and uncorrected images are both shown (left panel). LIF Intensities are calibrated using Chemkin Premix 1-D flame calculations.

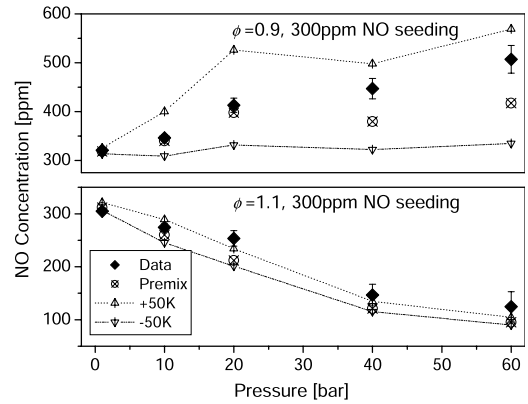


Fig. 7. Comparison of NO concentrations 3 mm above the burner matrix with Chemkin Premix 1-D flame code (GRI-Mech 3.0) as a function of pressure and equivalence ratio ( $\phi = 0.9$  and 1.1) with 300 ppm NO seeding. Arrowhead markers show simulations using temperature profiles scaled  $\pm 50$  K.

Reaction Design). The calculation is constrained by the measured temperature as a function of height above the burner to account for heat loss to the burner. The needed temperature profiles are provided by the 2-D NO-LIF thermometry (Fig. 4). To demonstrate the temperature dependence of these calculations, the temperature profile is scaled  $\pm 50$  K from the peak value and the resulting calculations are shown as arrowhead markers in Fig. 7. It can be seen from these data that the NO concentration is much more temperature-dependent in a fuel-lean flame than in a rich one. In lean flames the production of NO is dominated by the Zeldovich mechanism (otherwise known as thermal NO), and this mechanism has a very large temperature dependence [25], whereas in fuel rich flames the NO concentration is dominated by the reburn reactions, which are much less temperature-dependent. While reaction mechanisms in GRI-Mech are not specifically optimized for use in high-pressure conditions, the simulations show good agreement with experimental data when uncertainties in the temperature profile ( $\pm 50$  K) are considered.

#### 4.3. Pressure dependence of NO-LIF SNR

Spectrally resolved 1-D line-imaging offers unique advantages in applying single-shot detection of NO-LIF to practical systems. In the current work, 1-D line-imaging measurements were carried out for all flame pressures (1–60 bar) and stoichiometry to provide guidelines for filter selection in the multi-window detection strategies used for 2-D measurements. These 1-D measurements do not require the laser beam to be spread into a sheet, and the higher laser energy intensity

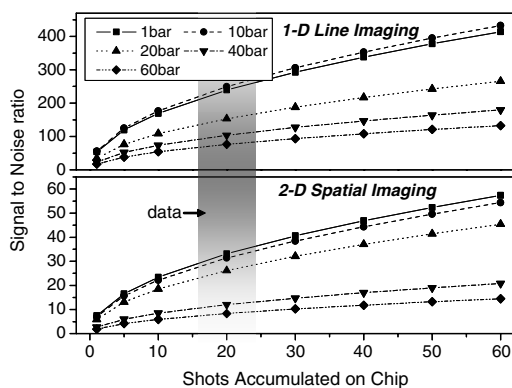


Fig. 8. Comparison of SNR for spectrally resolved 1-D imaging and 2-D imaging of NO-LIF for pressure conditions presented in this study (1–60 bar) and as a function of shots accumulated on chip (1 mJ/pulse).

results in increased SNR. A comparison of SNR for 1-D line and 2-D imaging data for 1 mJ laser energy used in the current study are presented in Fig. 8 for 300 ppm NO seeding. The curves in Fig. 8 were calibrated using data at 20 shots accumulated on chip and extended to other values using statistical arguments for this shot-noise-limited case. Averaging 20 shots is equivalent for our experimental setup to single-pulse laser energy of  $\sim 20$  mJ, a value generally recommended for single-shot 2-D imaging applications to achieve SNR of  $\sim 10$  at pressures exceeding 40 bar (assuming laser sheet of  $0.5 \times 15$  mm). Lasers are available commercially for these high powers, and as discussed above the excitation is well below saturation at elevated pressures. The high SNR of 1-D line-imaging and the added

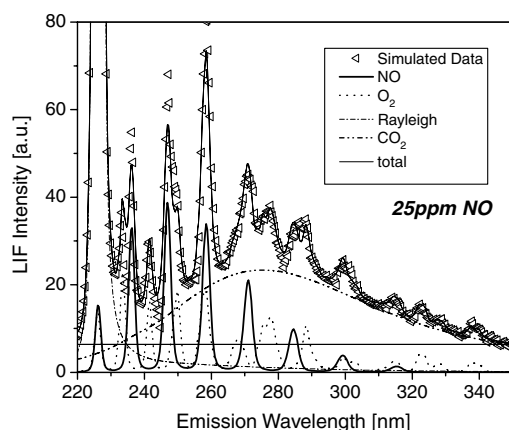


Fig. 9. Simulated 40 bar emission spectra with low NO concentration ( $\sim 25$  ppm). NO-LIF intensity is scaled using quantitative values obtained from this study. This method is applicable along a line in the path of the laser (1-D line-imaging).

benefit of monitoring multiple emission features of NO-LIF simultaneously offer high sensitivity to extremely low concentrations of NO. We can use present results to predict performance at lower NO concentrations using spectrally resolved 1-D imaging. Figure 9 shows a simulated fluorescence spectrum at 40 bar with a low (25 ppm) level of NO. NO-LIF features are clearly visible, though significant interference from  $O_2$  and  $CO_2$  can also be observed. Further studies to identify the minimum detectable NO concentrations using 1-D line-imaging are underway.

## 5. Conclusions

We have demonstrated a strategy for selective and quantitative LIF detection of NO in high-pressure combustion environments using spectrally resolved 1-D imaging and spatially resolved 2-D imaging (i.e., PLIF). A 2-D NO-LIF imaging strategy for high-pressure detection was proposed and demonstrated using multiple wavelength windows. Spectrally resolved 1-D line-imaging was used to identify the sources of interference and provide guidelines for selecting filters in the multi-window strategy. 2-D imaging of NO-LIF was demonstrated by using  $A-X(0,0)$  excitation (226.03 nm) with multi-window detection to correct for interference effects from other species ( $O_2$  and  $CO_2$ ) in slightly lean and rich conditions ( $\phi = 0.9$  and 1.1). In addition to imaging quantified concentrations of NO, the simultaneous imaging of the interference species  $O_2$  and  $CO_2$  is demonstrated. Spectrally resolved 1-D line-imaging offers the possibility of highly selective detection of NO-LIF down to extremely low concentrations ( $< 10$  ppm) with only a one-laser and one-camera setup. The discussions and demonstrations reported in this study provide a practical guideline for application of instantaneous 1-D or 2-D NO-LIF imaging in high-pressure combustion systems.

## Acknowledgments

This work was supported by the US Air Force Office of Scientific Research, Aerospace Sciences Directorate, with Julian Tishkoff as the technical monitor, and via an AFOSR STTR with Los Gatos Research. We acknowledge discussions and previous collaborations with Prof. C. Schulz (IVG, University of Duisburg) and Dr. Wolfgang G. Bessler (IWR, University of Heidelberg). In addition, we thank Dr. Bessler for spectral separation codes which were modified for use in this study. We thank Prof. C.T. Bowman of Stanford for his advice on flame chemistry model calculations.

## References

- [1] A.C. Eckbreth, *Laser Diagnostics for Combustion Temperature and Species*, Gordon and Breach, Amsterdam, 1996.
- [2] J. Wolfrum, *Proc. Combust. Inst.* 27 (1998) 1–41.
- [3] C.T. Bowman, in: C. Vovelle (Ed.), *Pollutants from Combustion*, Kluwer Academic Publishers, The Netherlands, 2000, pp. 123–144.
- [4] J. Warnatz, U. Maas, R.W. Dibble, *Combustion*, Springer, Berlin–Heidelberg–New York, 1997.
- [5] J.E. Dec, R.E. Canaan, SAE Tech. Paper Series 900147 (1998).
- [6] P. Jamette, P. Desgroux, V. Ricordeau, B. Deschamps, SAE Tech. Paper Series 2001-01-1926 (2001).
- [7] C. Schulz, V. Sick, U.E. Meier, J. Heinze, W. Stricker, *Appl. Opt.* 38 (1999) 1434–1443.
- [8] P. Andresen, G. Meijer, H. Schluter, H. Voges, A. Koch, W. Hentschel, W. Oppermann, W. Rothe, *Appl. Opt.* 29 (1990) 2392–2404.
- [9] A.O. Vyrodov, J. Heinze, M. Dillman, U.E. Meier, W. Stricker, *Appl. Phys. B* 61 (1995) 409–414.
- [10] M.D. DiRosa, K.G. Klavuhn, R.K. Hanson, *Comb. Sci. Tech.* 118 (1996) 257–283.
- [11] W.P. Patridge, M.S. Klassen, D.D. Thomsen, N.M. Laurendeau, *Appl. Phys. B* 34 (1996) 4890–4904.
- [12] D.D. Thomsen, F.F. Kuligowski, N.M. Laurendeau, *Appl. Opt.* 36 (1997) 3244–3252.
- [13] W.G. Bessler, C. Schulz, T. Lee, J.B. Jeffries, R.K. Hanson, *Appl. Opt.* 41 (2002) 3547–3557.
- [14] W.G. Bessler, C. Schulz, T. Lee, J.B. Jeffries, R.K. Hanson, *Appl. Opt.* 42 (2003) 2031–2042.
- [15] W.G. Bessler, C. Schulz, T. Lee, J.B. Jeffries, R.K. Hanson, *Appl. Opt.* 42 (2003) 4922–4936.
- [16] C. Schulz, J.D. Koch, D.F. Davidson, J.B. Jeffries, R.K. Hanson, *Chem. Phys. Lett.* 355 (2002) 82–88.
- [17] C. Schulz, J.B. Jeffries, D.F. Davidson, J.D. Koch, J. Wolfrum, R.K. Hanson, *Proc. Combust. Inst.* 29 (2002) 2725–2742.
- [18] W.G. Bessler, C. Schulz, T. Lee, J.B. Jeffries, R.K. Hanson, *Chem. Phys. Lett.* 375 (2003) 344–349.
- [19] W.G. Bessler, C. Schulz, V. Sick, J.W. Daily, in: 3rd Joint Meeting US Sec. Combust. Inst., Chicago available at (<www.lifsim.com>), 2003.
- [20] M. Tamura, J. Luque, J.E. Harrington, P.A. Berg, G.P. Smith, J.B. Jeffries, D.R. Crosley, *Appl. Phys. B* 66 (1998) 503–510.
- [21] F. Hildenbrand, C. Schulz, J. Wolfrum, F. Keller, E. Wagner, *Proc. Combust. Inst.* 28 (2000) 1137–1144.
- [22] P.A. Berg, G.P. Smith, J.B. Jeffries, D.R. Crosley, *Proc. Combust. Inst.* 27 (1998) 1377–1384.
- [23] G. Suck, J. Jakobs, S. Nicklitzsch, T. Lee, W.G. Bessler, M. Hofmann, F. Zimmermann, C. Schulz, SAE International (2004) 2004-01-1918.
- [24] T. Lee, W.G. Bessler, H. Kronmayer, C. Schulz, J.B. Jeffries, *Appl. Opt.* 44 (2005) 6718–6728.
- [25] Y. Zeldovich, *Acta Physicochimica USSR* 21 (1946) 577–628.

## Comments

*Alan Eckbreth, Consultant, USA.* Based on your work, what do you believe the single pulse, 2-D NO detection sensitivity to be in a turbulent, 30–40 bar combustor?

*Reply.* The 2D single-shot detection sensitivity of NO will depend on the experimental condition (i.e., laser power, detector efficiency and combustor conditions). For the well-defined laminar flame used in this study, we have observed a signal-to-noise ratio of  $\sim 12$  in a 40 bar flame with an NO concentration of  $\sim 450$  ppm. For the measurement strategies described here and a modest increase in laser pulse energy, we anticipate a detection sensitivity of  $\sim 50$  ppm or less in a 40 bar turbulent flame.

*Jerry Seitzman, Georgia Institute of Technology, USA.* What are the issues of making quantitative NO measurements at high pressure due to CO<sub>2</sub> and H<sub>2</sub>O absorption along a path where you don't have *a priori* information on the CO<sub>2</sub>/H<sub>2</sub>O/temperature profile along the laser path?

*Reply.* Correction for UV laser and signal attenuation in high-pressure combustors requires at least an estimate of the CO<sub>2</sub>, H<sub>2</sub>O and temperature ([16] in the paper), although for the excitation/detection wavelengths used and for temperatures in typical combustion environments, CO<sub>2</sub> is the dominant of the two interfering species (>95%). This attenuation correction only

requires an estimate of the temperature and the CO<sub>2</sub> concentration for relatively accurate (10%) corrections (remember the CO<sub>2</sub> absorption cross section increases with temperature). In addition, when multi-spectral detection is available, additional spectral regions which are optimized for CO<sub>2</sub> can provide a measurement of the CO<sub>2</sub> and this information can be used to estimate the concentration of CO<sub>2</sub>.

*Katharina Kohse-Höinghaus, Universität Bielefeld, Germany.* With respect to your choice of spectral regions for a multi-wavelength detection, would your study suggest a different optimization for applications in gas turbines or in engines, and how much is an effect of equivalence ratio versus that of pressure?

*Reply.* For engines and gas turbines which operate fuel-lean well, the optimization presented here should be quite good. For rich operating systems or those with stratified operation, emission spectra of the combustion gases should be examined (i.e., 1-D spectrally dispersed line imaging) after which additional optimization may be useful. It should also be noted that for the latter case, additional interference from PAHs or other compounds can be anticipated in which case alternative optimization or addition of even more spectral regions may be required.